Combustion and Flame
6/20/13

Lennard-Jones parameters for combustion and chemical kinetics modeling from full-dimensional intermolecular potentials

Ahren W. Jasper[a] and James A. Miller[b]

[a]*Combustion Research Facility, Sandia National Laboratories, PO Box 969, Livermore, CA 94551-0969, USA*
[b]*Chemical Sciences and Engineering Division, Argonne National Laboratory, Argonne, IL 60439, USA*

Abstract. Lennard-Jones parameters for use in combustion modeling, as transport parameters and in pressure-dependent rate-coefficient calculations as collision rate parameters, are calculated from accurate full-dimensional intermolecular potentials. Several first-principles theoretical methods are considered. In the simplest approach, the intermolecular potential is isotropically averaged and used to determine Lennard-Jones parameters. This method works well for small species, but it is not suitable for larger species due to unphysical averaging over the repulsive wall. Another method considered is based on full-dimensional trajectory calculations of binary collisions. This method is found to be very accurate, predicting Lennard-Jones collision rates within ~10% of those obtained via tabulated (experimentally-based) Lennard-Jones parameters. Finally, a computationally efficient method is presented based on one-dimensional minimizations averaged over the colliding partners' relative orientations. This method is shown to be both accurate and efficient. The good accuracy of the latter two approaches is shown to be a result of their explicit treatment of anisotropy. The effects of finite temperature vibrations and multiple conformers are quantified and are shown to be small. The choice of potential energy surface has a somewhat larger effect, and strategies based both on efficient semiempirical methods and on first-principles direct dynamics are considered. Overall, 75 systems are considered, including seven baths, targets as large as heptane, both molecules and radicals, and both hydrocarbons and oxygenates.

Keywords: Lennard-Jones parameters, anisotropy, intermolecular potential, ab initio, quantum chemistry

1. Introduction

Non-bonding intermolecular potentials play an important role in combustion chemistry. First and foremost (from our point of view), they govern collisional energy transfer from highly vibrationally excited molecules. In turn, this energy transfer largely controls the rates of unimolecular reactions at low pressure, both thermal and chemically-activated—most notably the low-pressure-limit rate coefficients of thermal dissociation reactions. However, these same potentials also determine transport properties—the coefficients of diffusion, viscosity, heat conduction, and thermal diffusion—that are used in flame modeling.[1,2] Although some work has appeared in these areas relatively recently,[3] there is still a dearth of information that can be applied directly in chemical kinetics and combustion modeling.

In two recent papers,[4,5] we have shown that a relatively inexpensive electronic-structure method, MP2/aug'-cc-pVDZ, gives results for intermolecular potentials that are very close to those calculated from the high-level QCISD(T)/CBS method for CH_4 interacting with several small-molecule bath gases (He, Ne, H_2, and CH_4). Furthermore, we parameterized a very efficient semiempirical potential energy surface for hydrocarbons interacting with typical atomic and diatomic baths based on the QCISD(T)/CBS interaction energies. Using these potentials we calculated energy transfer rates using trajectories that give accurate low-pressure rate coefficients for the CH_4 (+ M) ⇄ CH_3 + H (+ M) reaction, with M being any one of several typical bath gas molecules. Subsequent work (as yet unpublished for CH_4 + H_2O, CH_3OH + He, and C_xH_y + M) has reinforced our conclusion that the MP2 and semiemprical methodologies can be workhorses for obtaining collisional energy transfer rates in highly vibrationally-excited molecules, and hence accurate unimolecular rate coefficients at low pressure.

The purpose of the present investigation is considerably less ambitious than that described above, but it is still important. We want to use the intermolecular potential energy methods discussed above to calculate accurate Lennard-Jones collision rates (or frequencies) with minimal computational effort. In unimolecular reaction rate theory,[6,7] one is always referring to $\langle \Delta E \rangle$ or $\langle \Delta E_d \rangle$, the average energy transferred in a collision or the average energy transferred in a deactivating collision. For these quantities to have meaning one must first define what a collision is. There is enormous flexibility in this

definition,[8,9] but by convention it is normally defined in terms of a Lennard-Jones collision rate, which must be determined accurately. The origin of the use of the Lennard-Jones collision rate lies in the theory of transport processes. It is worthwhile to review this point briefly.

First, if one has a binary mixture of hard-sphere molecules, the collision rate of a molecule of species *i* with molecules of species *j* is[1]

$$Z_{ij} = \pi\sigma_{ij}^2 n_j \bar{g}_{ij} \ , \tag{1}$$

where n_j is the number density of *j*-type molecules; $\bar{g}_{ij} = \left(\frac{8k_BT}{\pi\mu_{ij}}\right)^{1/2}$ is the average relative speed for i, j collisions; k_B is Boltzmann's constant; $\mu_{ij} = \frac{m_i m_j}{m_i + m_j}$ is the reduced mass for i, j collisions; T is the temperature; and $\sigma_{ij} = \frac{1}{2}(\sigma_i + \sigma_j)$ is the collision diameter (with σ_i and σ_j the diameters of the two spheres). More generally, we will define σ_{ij} as the point where the intermolecular potential $\bar{V}(r)$ intersects the r axis—this is the collision diameter for hard spheres. In the same hard-sphere model the binary diffusion coefficient is

$$D_{ij} = \frac{3}{16}\frac{(2\pi k_B^3 T^3/\mu_{ij})^{1/2}}{p\pi\sigma_{ij}^2} \ , \tag{2}$$

where p is the pressure. Defining $z_{ij} = Z_{ij}/n_j$ to be a hard-sphere "collision rate coefficient", the diffusion coefficient becomes

$$D_{ij} = \frac{3}{16}\frac{\bar{g}_{ij}(2\pi k_B^3 T^3/\mu_{ij})^{1/2}}{pz_{ij}} . \tag{3}$$

Thus all of the dependence of D_{ij} on the potential is absorbed into z_{ij}.

If one considers the Lennard-Jones potential,

$$\bar{V}(r) = 4\varepsilon_{ij}\left[\left(\frac{\sigma_{ij}}{r}\right)^{12} - \left(\frac{\sigma_{ij}}{r}\right)^{6}\right], \tag{4}$$

where σ_{ij} was defined above and ε_{ij} is the well depth [or any potential of the form $\bar{V}(r) = \varepsilon f(r/\sigma)$], the diffusion coefficient can be written as

$$D_{ij} = \frac{3}{16} \frac{(2\pi k_B^3 T^3 / \mu_{ij})^{1/2}}{p\pi\sigma_{ij}^2 \Omega^{(1,1)*}} \tag{5}$$

where $\Omega^{(1,1)*}$ is a reduced collision integral that depends on the intermolecular potential. Equation (5) suggests that, by analogy with the hard-sphere case, we define the collision rate coefficient as

$$z_{ij} = \pi\sigma_{ij}^2 \Omega^{(1,1)*} \bar{g}_{ij} \tag{6}$$

One can view this as a general result with σ_{ij} and $\Omega^{(1,1)*}$ evaluated for the particular potential under consideration ($\Omega^{(1,1)*} = 1$ for hard spheres). Results analogous to Eq. (6) can also be derived using the viscosity and conductivity,[1] but in these cases $\Omega^{(2,2)*}$, another reduced collision integral, replaces $\Omega^{(1,1)*}$. We shall not be concerned with the precise definition of the collision integrals here except to note that their values are readily obtainable in tabular form. We are most interested in diffusion coefficients and hence in $\Omega^{(1,1)*}$, but the Lennard-Jones potential parameters that we determine can be used to calculate any of the reduced collision integrals. $\Omega^{(1,1)*}$ and $\Omega^{(2,2)*}$ are usually very similar in magnitude, commonly differing by less than 10%.

One is tempted to think that this is all well and good, but real molecules are not point particles (or hard spheres). They have structure—their potential depends on more than just the distance between the centers of mass of the two colliding molecules. Interestingly, high level quantum scattering calculations on *ab initio* potential energy surfaces show that transport properties can be computed quite accurately by using only the "spherically-averaged," isotropic part of the potential, i.e. by assuming point particles, at least for small molecules.[10,11,12] Also, the decades-old practice of fitting experimental data to Lennard-Jones potentials suggests that this simplification may be accurate.

In the present article we discuss different methods of obtaining Lennard-Jones parameters from detailed, full-dimensional intermolecular potentials. We compare the results with the experimental results available, normally by comparing collision rate coefficients for the different sets of Lennard-Jones parameters. We primarily consider

cases where helium is one of the collision partners. This simplifies the electronic-structure calculations and eliminates any effects of dipole-dipole interactions. The pure-gas parameters can be determined from whatever combining rules one may wish to use, as discussed recently by Brown et al.[3]

We would be remiss if we did not mention evidence that the Lennard-Jones potential may be too repulsive at short distances, leading to the underprediction of some diffusion coefficients at high temperatures by ~20%.[13] Paul and Warnatz[14] suggest that an exponential repulsive part may be more appropriate at high temperatures. The present methodology could be generalized to obtain potential parameters for such a potential as well. However, for now the Lennard-Jones potential is still in common use, largely because it is the potential used in CHEMKIN.[15] Brown et al.[3] recommend the use of Lennard-Jones parameters in combustion modeling over more complicated forms, as well. We will limit ourselves to determining those parameters in the present article. We also want to note that transport properties, particularly thermal conductivity and viscosity, depend on some other molecular properties, most notably dipole moments and polarizabilities. These properties can be computed accurately using relatively low-level electronic structure methods. We hope to address this issue in the near future.

2. Theory

Here we describe several methods for calculating isotropically-averaged (i.e., spherically-averaged) intermolecular potentials and/or Lennard-Jones collision parameters for a molecule or radical (A) interacting with a bath gas atom or molecule (B). All of the methods involve averaging the full-dimensional anisotropic intermolecular potential, $V(\mathbf{R})$, in some way over the colliding species' relative orientation and internal structures. This is simpler than evaluating the collision integrals directly using the full anisotropic potential. Instead, Lennard-Jones collision rate coefficients, z, are obtained from the calculated Lennard-Jones parameters σ and ε using Eq. (6) with[6]

$$\Omega^{(1,1)*} \approx [0.7 + 0.52 \log_{10}(k_B T / \varepsilon)]^{-1}, \tag{7}$$

where the "*i,j*" subscripts have been suppressed.

The total geometry of the interacting binary A + B system can be written as $\mathbf{R} \equiv (\mathbf{R}^{\mathrm{A}}, \mathbf{R}^{\mathrm{B}}, \mathbf{R}^{\Omega}, r)$, where $\mathbf{R}^{\mathrm{A}}$ labels the internal coordinates of the target species, $\mathbf{R}^{\mathrm{B}}$

labels the internal coordinates of the bath gas (if any), and the remaining coordinates define the relative orientation of the target and bath, $\mathbf{R}^{\Omega}$, and their center-of-mass separation, r. The full-dimensional intermolecular potential is defined relative to the separated *unrelaxed* species, i.e.,

$$V(\mathbf{R}) = E(\mathbf{R}) - E^{A}(\mathbf{R}^{A}) - E^{B}(\mathbf{R}^{B}), \tag{8}$$

where $E(\mathbf{R})$ is the total energy of the interacting target and bath gas evaluated at $\mathbf{R}$, $E^{A}(\mathbf{R}^{A})$ is the energy of the isolated target molecule or radical evaluated at $\mathbf{R}^{A}$, and $E^{B}(\mathbf{R}^{B})$ is the energy of the isolated bath gas atom or molecule evaluated at $\mathbf{R}^{B}$ (which for atomic baths is zero).

We consider two methods for calculating effective isotropic potentials. In the simplest scheme, the internal structures of the target and bath are set to their experimental or calculated equilibrium geometries, $\mathbf{R}^{A}_{eq}$ and $\mathbf{R}^{B}_{eq}$, and $V(\mathbf{R})$ is averaged over $\mathbf{R}^{\Omega}$ at fixed r. The isotropically-averaged potential is then

$$\bar{V}(r) = \sum_{n=1,N} V(\mathbf{R}^{\mathbf{A}}_{\mathbf{eq}}, \mathbf{R}^{\mathbf{B}}_{\mathbf{eq}}, \mathbf{R}^{\Omega}_{(n)}, r) / N, \tag{9}$$

where n labels the N uniformly sampled orientations for each r. At finite temperatures, the target and bath are not confined to their equilibrium structures.[16] Equation (9) can be modified to include this effect by sampling the internal configurations of the A and B from thermal distributions as we sample over relative orientations, i.e.,

$$\bar{V}(r) = \sum_{n=1,N} V(\mathbf{R}^{\mathbf{A}}_{(n)}, \mathbf{R}^{\mathbf{B}}_{(n)}, \mathbf{R}^{\Omega}_{(n)}, r) / N. \tag{10}$$

Equation (9) may be considered the low temperature limit of Eq. (10). Generally, Eq. (10) will predict longer-ranged interactions due to the effect of anharmonic vibrations. Even at elevated temperatures, however, one may expect Eqs. (9) and (10) to predict very similar effective isotropic potentials for small molecules and for larger molecules that do not feature large amplitude motions. Only for systems with multiple low-lying conformers with different shapes (long chain species with conformers related via torsions, for example) would one expect the effective anisotropic potential to depend non-negligibly on temperature; for such systems Eq. (10) may differ from Eq. (9).

The desired Lennard-Jones parameters can be determined straightforwardly from the isotropically-averaged potentials, with

$$\varepsilon = -\min_r \bar{V} \tag{11a}$$

$$\bar{V}(\sigma) = 0, \tag{11b}$$

where the second equation sets σ as the inner turning point of $\bar{V}$ evaluated at its asymptotic energy. Equation (11) requires locating two critical points on $\bar{V}$: its minimum and its inner turning point. It may be more convenient again to set

$$\varepsilon = -\min_r \bar{V} \tag{12a}$$

but then to use the associated value of r, $r_{\min}$, to approximate

$$\sigma = 2^{-1/6} r_{\min}. \tag{12b}$$

If the calculated isotropic potentials defined by Eqs. (9) and (10) were in fact Lennard-Jones potentials, then Eqs. (11) and (12) would be entirely equivalent. The difference in the predicted values of σ using Eqs. (11) and (12) is therefore one measure of the deviation of $\bar{V}$ from the Lennard-Jones form.

In the applications reported below, Eqs. (9) and (10) were evaluated for several normal alkane + He systems with N = 2000–10000 for each r. For Eq. (10), $\mathbf{R}^{\mathrm{A}}_{(n)}$ was sampled from thermal distributions of geometries determined via separate molecular dynamics calculations subject to an Andersen thermostat.[17] In addition to reporting $\bar{V}$, we also report the minimum and maximum value of V sampled for each r. These extrema provide a measure of the anisotropy of V.

Next we consider using classical trajectories to calculate Lennard-Jones parameters directly,[18] i.e., not in reference to an isotropically-averaged intermolecular potential. In this approach, a small ensemble of target–bath gas collisions is prepared using initial conditions appropriate for collisional energy transfer calculations,[4,5] subject to the additional constraint of zero impact parameter. Along each trajectory n, the instantaneous value of V is monitored, and the most negative value of V encountered, V_n, and its associated center-of-mass distance, r_n, are recorded. The trajectory-based Lennard-Jones parameters are then defined

$$\varepsilon = -\sum_{n=1,N} V_n / N. \tag{13a}$$

$$\sigma = 2^{-1/6} \sum_{n=1,N} r_n / N. \tag{13b}$$

This approach for calculating σ and ε differs in several ways from the use of Eqs. (9) and (10). First, the target and bath are vibrating during the full-dimensional trajectory collisions, and these internal motions may, in general, react to the presence of the other species during the collision; i.e., the trajectory interactions are "softer" and include dynamical effects due to the collision that are not available to the static sampling and averaging approaches described by Eqs. (9) and (10). Second, the trajectory-based Lennard-Jones parameters are derived directly from the full-dimensional (anisotropic) potential, whereas in Eqs. (9) and (10) the anisotropy is averaged over *before* the Lennard-Jones parameters are determined. If the intermolecular potential were really isotropic and if the dynamical effect of internal vibrations were small, the two approaches would give similar results. The trajectory-based Lennard-Jones parameters therefore include anisotropic effects that are not included in Eqs. (9) and (10) and may be considered "effective" Lennard-Jones parameters that include this anisotropy. Finally, the trajectories are subject to total energy constraints, and so the trajectory method never samples highly repulsive interactions, whereas the isotropically averaged potentials in Eqs. (9) and (10) will generally include contributions from geometries high on the repulsive wall, even for r close to the minimum of the effective isotropic potential.

Full-dimensional molecular dynamics may be too expensive for practical evaluations of Lennard-Jones parameters, and a somewhat simpler approach is considered next. However, when one requires Lennard-Jones parameters to be used alongside molecular dynamics studies of energy transfer, the present ensembles represent a small fraction of the total cost of such a calculation.

We also note that one could use classical trajectories to calculate transport properties.[19,20] An advantage of such an approach would be that one could avoid assuming the isotropic Lennard-Jones form (or some other simplified form) for the intermolecular potential. The goal of the present work is to validate convenient schemes for obtaining transport and collisional parameters for use in building detailed models of combustion and for pressure-dependent reaction rate coefficients, where, as discussed above, it is both conventional and expedient to assume Lennard-Jones interactions. We therefore do not consider using full-dimensional trajectories to calculate transport properties directly in this work.

Finally, we present a method that includes the effect of local anisotropy, as in the trajectory-based method, but that does not require full-dimensional trajectories. This method incorporates desirable aspects of both of the approaches described above. In the simplest implementation, $\mathbf{R}_\Omega$ is sampled uniformly and $V(\mathbf{R}_{\mathrm{eq}}^{\mathrm{A}}, \mathbf{R}_{\mathrm{eq}}^{\mathrm{B}}, \mathbf{R}_{(n)}^{\Omega}, r)$ is minimized with respect to r, and

$$\frac{d}{dr} V(\mathbf{R}_{\mathbf{eq}}^{\mathbf{A}}, \mathbf{R}_{\mathbf{eq}}^{\mathbf{B}}, \mathbf{R}_{(n)}^{\Omega}, r) = 0\,, \tag{14}$$

defines the values of V_n and r_n. Lennard-Jones parameters are then calculated via Eq. (13). Alternatively, one can perform an additional optimization to locate the inner turning point, σ_n, for each $\mathbf{R}_{(n)}^{\Omega}$ and calculate

$$\varepsilon = -\sum_{n=1,N} V_n / N\,. \tag{15a}$$

$$\sigma = \sum_{n=1,N} \sigma_n / N\,. \tag{15b}$$

Finally, we note that one could sample over the internal geometries of the target and bath gas along with the orientations, where V_n and r_n are then obtained by minimizing $V(\mathbf{R}_{(n)}^{\mathrm{A}}, \mathbf{R}_{(n)}^{\mathrm{B}}, \mathbf{R}_{(n)}^{\Omega}, r)$ with respect to r,

$$\frac{d}{dr} V(\mathbf{R}_{(n)}^{\mathbf{A}}, \mathbf{R}_{(n)}^{\mathbf{B}}, \mathbf{R}_{(n)}^{\Omega}, r) = 0\,. \tag{16}$$

Such an approach includes temperature and multiconformational effects, as discussed above for Eq. (10).

As with the trajectory approach, the one-dimensional-minimization approach results in effective Lennard-Jones parameters that include anisotropy. The present method differs from the trajectory method in that it is much less computationally demanding, with the tradeoff that dynamical collision effects are not included.

The results of any of the methods described above will depend sensitively on the potential energy surface used. Several potential energy surfaces have been considered here, including both direct dynamics and more efficient approximate representations. For hydrocarbons targets, we make use of our recently developed analytic intermolecular potential energy surfaces,[5] which have been validated against high-level QCISD(T)/CBS energy calculations as well as in dynamical calculations of energy transfer. These

potential energy surfaces (labeled "exp/6") employ a tight binding model[21] to describe the internal potential of the target along with parameterized "separable pairwise" Buckingham (i.e., exp/6) interactions for the target–bath atomic interactions. Buckingham parameters for several baths are taken from Refs. 5 and 22. For targets containing oxygen atoms and to further test the exp/6 parameterization for hydrocarbons, we also consider high-level direct MP2/CBS and QCISD(T)/CBS calculations with counterpoise corrections and CBS extrapolations based on aug-cc-pVDZ and aug-cc-pVTZ basis sets. (One expects the more widely used and slightly more computationally expensive CCSD(T) method to perform similarly to the QCISD(T) method.) Finally, we test the accuracy of less expensive direct dynamics methods, including (briefly) DFT and MP2 with small and medium-sized basis sets and our previously employed[4,5] MP2/aug'-cc-pVDZ potential.

The calculated binary Lennard-Jones parameters and collision rates are compared with tabulated values collected from a variety of sources. The usual combining rules are used, with the arithmetic mean used for σ and the geometric mean used for ε. Pure gas values for the bath gases are taken principally from the tables distributed with CHEMKIN,[15] with Ne and Kr from Ref. 23: σ = 2.576, 2.749, 3.330, 3.684, 2.920, 3.681, 3.458 Å and ε = 7.098, 24.74, 94.87, 121.4, 26.41, 67.89, 74.64 cm^{-1} for He, Ne, Ar, Kr, H_2, N_2, and O_2, respectively. Parameters for several normal alkanes are taken from Tee et al.[24] and are based on experimental viscosities and second virial coefficients. Hexane is not included in this tabulation, so its values are linearly interpolated from pentane and heptane. Parameters for the other target molecules and radicals are taken from CHEMKIN's distributed tables.[15]

3. Results and discussion

3.1. Isotropically averaged potentials

The exp/6 potential was used to evaluate the isotropically averaged potentials described by Eqs. (9) and (10) with N = 10000 for four normal alkanes + He, with the resulting Lennard-Jones parameters summarized in Table 1. The isotropically-averaged potentials defined by Eq. (9) are plotted in Fig. 1 for methane, ethane, and butane + He, where it can be seen that the potentials are well described by the Lennard-Jones form.

The calculated values of σ obtained via Eqs. (11) and (12) differ negligibly for CH_4 and only by 4% for hexane, which supports the use of this functional form to describe the isotropically-averaged intermolecular potential, at least for the region of the potential near the well and inner turning point. One can notice some minor deviations from the Lennard-Jones form at longer and shorter distances, particularly for the larger species.

Using Eq. (9), the calculated values of σ^2 (the square of σ is proportional to the collision rate, as shown in Eq. (6)) are larger than the tabulated ones by only 17% for methane but by more than 100% for hexane, while the calculated values of ε are smaller by 30–80%. Because the deviations from the tabulated values for these two parameters are in different directions, these effects cancel somewhat when calculating the collision rates. For example, for CH_4 + He σ^2 and ε differ from the tabulated values by +17% and –30%, while the collision rates differ by only 10%.

Agreement with the tabulated collision rates is worse for the larger systems, principally due to significant differences between the calculated and tabulated values of σ. Furthermore, while the tabulated well depths ε increase almost linearly with size, the calculated ones are similar for methane, ethane, and butane, and the calculated value of ε for hexane is *smaller* than for the smaller species. These differences can be explained by considering the anisotropy in the intermolecular potential, as indicated by minimum and maximum sampled values of V shown in Fig. 1. Even for the smallest system considered, CH_4 + He (Fig. 1(a)), there is significant anisotropy in the potential for $r < 4$ Å. At the inner turning point on $\bar{V}$ ($r = 3.38$ Å) for example, the minimum and maximum energies on the anisotropic potential differ by 100 cm^{-1}, which is 4x as large as ε. This suggests that, even for a small and roughly spherical system like CH_4 + He, one may expect significant anisotropy and that predicted Lennard-Jones parameters will be sensitive to the treatment of this anisotropy. Similarly, we note that the locations of the inner turning points along the most and least attractive approaches for CH_4 + He differ by almost 1 Å.

As may be expected, there is even more anisotropy for the larger species. For C_2H_6 + He, one can identify two groups of approaches in the minimum-energy curve in Fig. 1(b): one with a minimum near $r = 4.2$ Å that includes approaches to the $–CH_3$ ends of ethane with interactions similar in magnitude to the CH_4 + He interactions, and one with a minimum near $r = 3.5$ Å that includes shorter-ranged and more attractive

interactions as He approaches perpendicularly to the C–C axis of ethane. These two types of approaches lead to even greater anisotropy for ethane than for methane. For butane, there are more than two qualitatively different types of approaches, but we do not attempt to enumerate them. Instead, we note that the variation in the locations of the inner turning points for the most and least attractive approaches for butane + He is 2.3 Å!

This significant anisotropy explains the inaccuracy of Eq. (9) for large systems. For example, when sampling over the butane + He interactions at the tabulated value of σ = 3.8 Å, the averaged potential includes geometries very high up on the repulsive wall—as high as 35,000 cm^{-1}. For large enough molecules, these energies can be made arbitrarily large, because the bath gas atom may be put arbitrarily close to an atom on the target molecule. The isotropic potentials obtained via Eq. (9) are therefore contaminated by the resulting "infinities." As a practical matter, the exp/6 potentials are not expected to be accurate so high up on the repulsive wall. Even if the potentials were accurate, it is formally undesirable that this region of the potential should contribute so significantly in determining the transport properties. Most importantly, perhaps, the use of Eq. (9), while accurate for small systems, significantly overpredicts the tabulated collision rates for butane and hexane. One may conclude that these overpredictions are due to inaccurate averaging over the repulsive wall, which leads to erroneously large values of σ.

We note another complication that arises for the normal alkanes larger than propane and more generally for any system with multiple conformers. Butane + He parameters were predicted via Eq. (9) for two equilibrium structures: one corresponding to the anti conformer of butane and one corresponding to the gauche conformer of butane. As seen in Fig. 1(c), the gauche conformer results in a shorter-ranged isotropically-averaged potential relative to that of the anti conformer and leads to collision rates that are ~10% smaller (as shown in Table 1). One may anticipate this effect to be more significant for larger systems. This ambiguity can be resolved by using the temperature-dependent method defined by Eq. (10). This method properly weights the two conformers according to their relative thermal populations. The drawback of this approach is that the predicted Lennard-Jones parameters are temperature dependent. Nonetheless, Eq. (10) may be useful for some systems. Even for systems without torsions, the effect of finite-temperature vibrations can be seen in Table 1. For methane

and ethane + He, the use of Eq. (10) leads to collision rates that are very similar at 300 K and that are only a few percent larger at 3000 K. We may conclude that—aside from multiple conformer effects—the effect of finite-temperature vibrations is small, even at high temperatures.

3.2. Effective parameters with anisotropy from full-dimensional trajectories

Ensembles of $N = 2000$ classical trajectories and the exp/6 potential were used as described in Sec. II to calculate Lennard-Jones parameters for a variety of normal hydrocarbons and for several atomic and diatomic baths. The results are compared with tabulated values in Table 2. Agreement is excellent when He is the bath gas, with the calculated Lennard-Jones collision rates differing from the tabulated ones typically by less than 3%. For the other baths, the predicted collision rates again agree well with the tabulated values, but the differences can be as large as 10%. The good agreement over this wide variety of baths and for targets as large as heptane is encouraging.

For He, the individual Lennard-Jones parameters are very similar to the tabulated values, with σ typically predicted within ~0.1 Å and ε predicted within a few cm^{-1}. For the other baths, the differences are somewhat larger, and the predicted collision rates benefit from the cancellation discussed above. Bastien et al.[25] have stressed that the experimental measurements cannot fix the two parameters individually and have instead identified a two-dimensional "trough" of suitable experimentally-inferred pairs of values for σ and ε. This trough can be defined through the collision rate, as discussed in the Introduction. The present differences in the individual parameters therefore do not necessarily indicate poor performance of the method. Again, the overall agreement in the predicted collision rates is very good.

Transport parameters are most often tabulated for use in kinetic modeling as pure gas (self-interaction) Lennard-Jones parameters, which are then converted to binary Lennard-Jones parameters via simple combining rules.[3,25] To make a practically useful list from the present results, the binary Lennard-Jones parameters calculated here would need first to be converted to a list of self-interaction parameters. To do this, one could assume some set of pure gas parameters for the bath gas and then calculate the pure gas parameters for the target species by inverting the combining rule, as noted in the

Introduction. The results in Table 2 can be used to test the sensitivity of the results of this procedure on the choice of the bath gas. Using tabulated parameters for the seven bath gases, the inferred pure gas values of σ for CH_4 vary from 3.17–3.83 Å and the inferred pure gas values of ε vary from 82–323 cm^{-1}. Notably, the largest value for σ and the smallest value for ε are obtained for He, and H_2 gives the smallest value for σ and the largest value for ε. Similar sensitivities are obtained for the larger alkanes. One cannot assign a preferred bath gas by comparison with tabulated values, as the tabulated values themselves require assuming a combining rule. Instead we note that N_2 is the most important collider in many applications, and its values are close to the mean of the ranges identified above. Furthermore, while the maximum deviation in σ is large for the different baths, the root-mean-squared deviation in σ is only 7% (15% in the collision rate). The relative deviation is larger for ε, but the collision rate is less sensitive to this parameter. In general, we recommend the use of N_2 as a collision partner when generating pure gas collision rates. Alternatively, one could directly calculate pure gas collision parameters. Often, however, these interaction potentials are not well known, and the appropriateness of the combining rules used in subsequent kinetic modeling would nonetheless remain in question.

The systems in Table 2 were selected to keep things manageable, but the trajectory method and the exp/6 potential may be readily applied to unsaturated hydrocarbon species and hydrocarbon radicals as well. This is demonstrated for ten C_3H_x + He systems in Table 3. There are clear trends with respect to the number of hydrogen atoms. The collision rates for the molecular species increase systematically with increasing saturation—by 7% for each pair of hydrogen atoms added. The two C_3H_4 isomers, allene and propyne, have similar collision rates. In practice and due to a general lack of information about radicals, radicals species are often assigned the collision parameters of related hydrogenated or dehydrogenated molecules. The present results suggest that it is a good approximation to adopt parameters of "nearby" hydrogenated molecules, although the radical species' collision rates are sometimes smaller by a few percent.

3.3. Effective parameters with anisotropy from one-dimensional minimizations

The exp/6 potential was used to perform one-dimensional minimizations, averaged over orientation, as described by Eqs. (14) and (16) with N = 2000 for four normal alkanes + He. The results are shown in Table 4. The predicted collision rates are within ~15% of the tabulated ones, and, unlike the isotropically-averaged potential methods, the accuracy of the one-dimensional minimization approach remains good for the larger systems. The one-dimensional minimization methods tend to overpredict the tabulated rates, and this overprediction does increase somewhat with size.

Figure 2 shows representative one-dimension cuts for three normal alkanes + He. The local minimum for each cut is indicated, and these values are averaged (for larger ensemble sizes than shown in Fig. 2) to obtain the results in Table 4. Figure 2 may be compared with Fig. 1. In Fig. 1, the potential is spherically averaged first, and then the Lennard-Jones parameters are extracted. In Fig. 2, Lennard-Jones parameters for each approach are determined first, and these are then averaged. Clearly, the latter approach incorporates anisotropic information not available to the former approach. The poor performance of the approach in Fig. 1 further demonstrates that local anisotropic information is required for quantitative predictions.

Also shown in Fig. 2 are representative results from the trajectory method discussed above. Note that while the trajectory approach results in values for V_n and r_n that are similar to those obtained via the one-dimensional minimizations, they are systematically shorter-ranged and more attractive. These differences may be attributed to dynamical effects not included in the one-dimensional minimizations. Specifically, the colliding partners experience "softer" interactions than the rigid fragment approaches due to vibrational deformations from the impact of the collisions.

There is relatively little sensitivity of the one-dimensinal minimization results on the temperature of the target, with the application of Eqs. (14) and (16) predicting rates differing by only a few percent. This is in contrast to the results shown in Table 1 for the isotropic potential methods. We can explain this result by noting that the one-dimensional minimizations depend only on the local (i.e., anisotropoic) potential, whereas the isotropic averages depend on the global potential for fixed r. The choice of conformer of

the target molecule therefore has more of an effect on the predictions of the isotropically-averaged methods in Table 1 than the one-dimensional minimization methods in Table 4.

The results in Table 4 are similar in overall accuracy to those predicted by the trajectory method in Tables 2 and 3. There are systematic differences, however. The trajectory method tends to underpredict the collision rates, whereas the one-dimensional minimization method overpredicts them. If we compare the finite temperature results in Table 4 with the trajectory results in Table 2, we can attribute the differences in the predictions to dynamical effects in the trajectory calculations. These differences vary from ~5% for methane to ~15% for hexane.

The one-dimensional minimizations are orders of magnitude less demanding computationally than the trajectory method and are simple to implement, particularly if Eq. (14) is used. We therefore recommend this approach as a practical method for obtaining accurate Lennard-Jones collision parameters.

3.4. Sensitivity to the potential energy surface

We also consider the sensitivity of the predicted results to the choice of potential energy surface. For these tests, we use the one-dimensional minimization method exclusively, with finite temperature effects neglected, i.e., we use Eq. (14). Results for several small systems + He are summarized in Table 5. Aside from relatively poor results for H + He and CH + He, all of the potentials considered predict collision rates in fairly good agreement with the tabulated values, typically within 15%. The larger differences for the lighter species and for H + He in particular may be due to the representation of the repulsive wall by the Lennard-Jones form.[13,14] The present calculated values for σ and ε for H + He agree with those based on the high level calculated potential energy surface of Middha et al.[13]

The QCISD(T)/CBS method is the highest-level method considered, and it is encouraging that it generally agrees with the somewhat less expensive MP2/CBS method. The much less expensive MP2/aug'-cc-pVDZ method often agrees with the higher-level methods, with differences as large as 10%. The exp/6 potential was originally parameterized[5,22] against QCISD(T)/CBS calculations for CH_4 + He but neglects nonpairwise interactions. Furthermore the exp/6 potential uses the CH_4 + He-based atom-

atom interaction parameters for all hydrocarbon interactions. We have not developed similarly general exp/6 parameters for oxygenates.

We emphasize that all of the potentials considered here may be expected to be fairly accurate, either as first-principles approaches (MP2/CBS and QCISD(T)/CBS) or because they have been previously validated against such high-level calculations (exp/6 and MP2/aug'-cc-pVDZ). To demonstrate the errors associated with choosing a *bad* potential, we obtained results using the B3LYP and M06-2X density functional theory methods. Both of these functionals have been successfully employed in a wide variety of contexts throughout chemistry, but neither is explicitly designed to treat dispersion interactions. The resulting Lennard-Jones parameters can by unphysical when these methods are used. For example, the M06-2X/cc-pVDZ method predicts $\varepsilon = 161$ cm^{-1} and $\sigma = 2.30$ Å for C + He, which are very different from the tabulated values of 18.8 cm^{-1} and 2.94 Å and the high level (QCISD(T)/CBS) calculated values of 19.5 cm^{-1} and 2.91 Å. The B3LYP/cc-pVDZ method also predicts innacurate values of $\varepsilon = 80.2$ cm^{-1} and $\sigma =$ 2.33 Å for C + He. Density functional theories designed specifically for dispersion interaction[26] were not tested here. Instead we note the general difficulty in predicting weak dispersion reactions and the good accuracy of the counterpoise corrected MP2 and QCISD(T)/CBS methods.

In general, the calculation of accurate intermolecular potentials requires the use of large augmented (diffuse) basis sets, basis set extrapolations, counterpoise corrections, and some post-Hartree–Fock approach, preferably with perturbative triples.[27] Less expensive potentials may accidentally perform well in predicting collision rates, however, due to the cancellation discussed above. When a less predictive method, say, overpredicts the strength of the interactions, it is almost certain also to be shorter-ranged, such that the two errors cancel.

Finally, results for several systems relevant to combustion are reported in Table 6 calculated using the MP2/CBS potential and Eq. (14). General agreement with tabulated collision rates is good, although there are notable exceptions. As noted above, the present approach overpredicts the H + He collision rate by 50%, which may be due to the treatment of the repulsive wall. The tabulated[15] pure gas value of σ for HCCO is 2.5 Å, which is much smaller than tabulated values of σ for related species. The predicted value

of σ for HCCO + He is 3.6 Å and is similar to other H_xC_2O species. This choice in the tabulated value of σ for HCCO leads to values of z_{calc}/z_{tab} close to 2 in Table 6 for HCCO + He. Otherwise, the predicted and tabulated collision rates typically differ by less than 20%.

4. Conclusions

Several methods for calculating binary Lennard-Jones collision parameters from full-dimensional intermolecular potentials have been considered. While orientationally averaging over real potentials does result in isotropically-averaged potentials that are well described by the Lennard-Jones form, collision rates based on these potentials are not accurate for systems larger than a few atoms. We demonstrated that, even for small molecules, real potentials feature significant anisotropy in the region of the potential relevant to transport. When orientationally averaging over real potentials, this anisotropy leads to unphysical averaging over repulsive interactions and significant errors in predicted transport parameters.

Two methods for calculating *effective* Lennard-Jones parameters directly from full-dimensional anisotropic intermoleculars potential were considered. The first involves small ensembles of full-dimensional trajectories and was shown to predict Lennard-Jones collision rates in excellent (10%) agreement with tabulated values for systems as large as heptane and for several baths. The predicted values of σ are typically smaller than the tabulated values, and the predicted values of ε are typically larger than the tabulated values. These two errors cancel when evaluating collision rates and therefore may not indicate poor performance of the method, as emphasized by Brown and co-workers.[3,25]

The second method for calculating effective Lennard-Jones parameters is much simpler and more computationally efficient than the trajectory approach and involves one-dimensional minimizations averaged over relative orientations of the two species. Again, agreement between the predicted and tabulated collision rates is excellent (10%). The trajectory method tends to underpredict the collision rates, while the one-dimensional minimization method tends to overpredict the collision rates. These systematic differences may be attributed to dynamical effects resulting in “softer” interactions in the trajectory approach.

In principle, one can include multiconformer effects and, more generally, the effect of temperature-dependent vibrations for the target and bath gas species for any of these methods tested here. The present tests confirm that such effects are small and may typically be neglected.

Both radical and molecular species were considered. The present results confirm that Lennard-Jones parameters for radical species may be accurately approximated as those of associated hydrogenated (+H) molecules. One can, however, identify a systematic increase in the predicted collision rates of molecular species with increasing saturation (+2H).

The consistency of simple combining rules (the arithmetic mean for σ and the geometric mean for ε) with the present results was tested for several normal alkanes and several baths. Pure gas Lennard-Jones parameters for the normal alkanes obtained from binary parameters depend fairly sensitively on the choice of bath gas. Notably, the use of He as the bath gas, systematically results in the largest pure gas normal alkane values for σ and the smallest values of ε. The use of N_2, on the other hand, results in pure gas normal alkane values of σ and ε close to their average values. Although He was primarily considered here, it may be more useful to use N_2 as the collision partner when compiling lists of transport parameters for use in modeling studies.

Finally, the sensitivity of the predicted parameters on the choice of the level of theory used to describe the potential energy surface was considered. The previously fitted semiempirical exp/6 intermolecular potential is found to be accurate, but its applicability is limited to hydrocarbons interacting with typical atomic and diatomic baths. For oxygenated species, two high level ab initio methods were considered: the counterpoise corrected MP2 and QCISD(T) methods with CBS basis set extrapolations. Typically the two methods were found to result in similar predictions. More approximate ab initio methods were also considered. While the previously employed MP2/aug'-cc-pVDZ method performed fairly well, other inexpensive ab intio methods including density functional theory were shown to lead to significant errors. Notably, these results again demonstrated the significant cancellation in the collision rate arising from opposite-sign errors in the predicted values of σ and ε.

The cumulative effect of the present predicted (typically) 0–20% changes to collision rates in Table 6 on various properties of combustion modeling is not known. The present approach provides not only a convenient means for obtaining transport properties for species not previously tabulated but also provides a means for obtaining a systematic set of transport properties. Such a systematic set may aid in future sensitivity analyses of transport properties in combustion modeling.

Acknowledgments

A. W. J. was supported by the Division of Chemical Sciences, Geosciences, and Biosciences, Office of Basic Energy Sciences, U.S. Department of Energy. Sandia is a multiprogram laboratory operated by Sandia Corporation, a Lockheed Martin Company, for the United States Department of Energy under Contract No. DE-AC04-94-AL85000. J. A. M. was supported under contract number DE-AC02-2006-CH11357 as part of the ASC-HPCC (ANL FWP #59044).

Table 1. Calculated Lennard-Jones parameters based on effective isotropic potentials compared with tabulated values and relative collision rates for four normal alkanes + He[a]

		Calculated[b]		Tabulated[c]		z_{calc}/z_{tab}		
Target	Method	σ, Å	ε, cm^{-1}	σ, Å	ε, cm^{-1}	300 K	1500 K	3000 K
CH_4	Eq. (9)	3.38	19.8	3.13	28.7	1.09	1.11	1.11
	Eq. (10)	3.39–3.43	19.6–18.7	3.13	28.7	1.09	1.12	1.14
C_2H_6	Eq. (9)	3.77	24.2	3.40	36.8	1.13	1.16	1.16
	Eq. (10)	3.79–3.85	23.8–22.3	3.40	36.8	1.14	1.17	1.20
C_4H_{10}	Eq. (9)[d]	4.73	19.0	3.79	44.3	1.32	1.37	1.39
	Eq. (9)[e]	4.46	24.4	3.79	44.3	1.23	1.26	1.28
	Eq. (10)	4.50–4.67	23.3–20.1	3.79	44.3	1.24	1.31	1.36
C_6H_{14}	Eq. (9)[d]	5.93	11.3	4.04	51.9	1.61	1.73	1.76
	Eq. (10)	5.88–5.74	11.7–12.2	4.04	51.9	1.59	1.66	1.67

[a]For the exp/6 intermolecular potential

[b]Via Eq. (11)

[c]From Ref. 24

[d]Anti conformer

[e]Gauche conformer

Table 2. Calculated Lennard-Jones parameters based on full-dimensional trajectories compared with tabulated values and relative collision rates for several normal hydrocarbons in several baths[a]

		Calculated		Tabulated[b]		z_{calc}/z_{tab}		
Target	Bath	σ, Å	ε, cm^{-1}	σ, Å	ε, cm^{-1}	300 K	1500 K	3000 K
CH_4	He	3.20	24.1	3.13	28.7	1.01	1.02	1.02
	Ne	3.25	53.7	3.21	53.6	1.02	1.02	1.02
	Ar	3.47	128	3.50	105	1.04	1.02	1.01
	Kr	3.51	163	3.68	119	1.00	0.97	0.96
	H_2	3.05	92.4	3.30	55.3	0.96	0.93	0.92
	N_2	3.59	122	3.68	88.7	1.04	1.01	1.00
	O_2	3.35	126	3.57	93.0	0.95	0.93	0.93
C_2H_6	He	3.36	36.3	3.40	36.8	0.97	0.97	0.97
	Ar	3.62	168	3.78	134	0.98	0.96	0.96
	N_2	3.78	148	3.95	114	0.98	0.96	0.95
C_3H_8	He	3.55	43.4	3.78	36.3	0.92	0.91	0.90
	Ar	3.80	194	4.16	133	0.94	0.90	0.90
	N_2	3.96	164	4.33	112	0.93	0.90	0.89
C_4H_{10}	He	3.71	48.3	3.79	44.3	0.98	0.97	0.97
	Ne	3.76	80.6	3.88	82.8	0.93	0.93	0.94
	Ar	3.95	214	4.17	162	0.98	0.95	0.94
	Kr	3.94	292	4.34	183	0.96	0.91	0.90
	H_2	3.67	147	3.96	85.6	0.99	0.95	0.94
	N_2	4.12	178	4.34	137	0.97	0.95	0.94
	O_2	3.86	240	4.23	144	0.97	0.92	0.91
C_5H_{12}	He	3.84	52.6	3.93	48.3	0.97	0.97	0.97
	Ar	4.04	235	4.31	177	0.96	0.93	0.93
	N_2	4.23	192	4.48	150	0.96	0.94	0.93
C_6H_{14}	He	3.96	56.4	4.04	51.9	0.98	0.97	0.97
	Ne	3.96	92.2	4.12	97.0	0.91	0.91	0.92
	Ar	4.16	251	4.41	190	0.97	0.94	0.94
	Kr	4.15	344	4.59	215	0.96	0.91	0.90
	H_2	3.90	166	4.21	100	0.99	0.95	0.93
	N_2	4.37	201	4.59	161	0.97	0.95	0.94
	O_2	4.10	288	4.48	169	1.00	0.94	0.92
C_7H_{16}	He	4.06	58.9	4.15	55.3	0.97	0.97	0.97
	Ar	4.24	265	4.52	202	0.96	0.93	0.93
	N_2	4.42	213	4.70	171	0.95	0.92	0.92

[a]For the exp/6 intermolecular potential

[b]From Refs. 15, 23, and 24

Table 3. Calculated Lennard-Jones parameters based on full-dimensional trajectories for C_3H_x + He compared with tabulated values for propane + He[a]

			z_{calc}/z_{tab}		
Target	σ, Å	ε, cm^{-1}	300 K	1500 K	3000 K
HCCC	3.20	42.1	0.74	0.73	0.73
HCCCH[b]	3.21	44.0	0.75	0.74	0.74
H_2CCCH	3.24	45.1	0.77	0.76	0.76
H_2CCCH_2	3.28	45.7	0.79	0.78	0.78
H_3CCCH	3.31	44.6	0.80	0.79	0.79
H_2CCHCH_2	3.35	44.7	0.82	0.81	0.81
H_3CCHCH_2	3.43	44.2	0.86	0.85	0.85
$H_3CCH_2CH_2$	3.56	41.8	0.91	0.90	0.90
H_3CCHCH_3	3.55	41.5	0.91	0.90	0.90
$H_3CCH_2CH_3$	3.55	43.5	0.92	0.91	0.90

[a]For the exp/6 intermolecular potential

[b]Hydrogenated "parent" molecules in bold may be compared with the associated radical(s) listed above them.

Table 4. Calculated Lennard-Jones parameters based on one-dimensional minimizations compared with tabulated values and relative collision rates for four normal alkanes + He[a]

		Calculated[b]		Tabulated[c]		z_{calc}/z_{tab}		
Target	Method	σ, Å	ε, cm^{-1}	σ, Å	ε, cm^{-1}	300 K	1500 K	3000 K
CH_4	Eq. (14)	3.32	21.5	3.13	28.7	1.07	1.08	1.09
	Eq. (16)	3.33–3.35	21.4–21.0	3.13	28.7	1.07	1.09	1.10
C_2H_6	Eq. (14)	3.64	28.9	3.40	36.8	1.08	1.10	1.10
	Eq. (16)	3.63–3.66	28.8–28.3	3.40	36.8	1.08	1.11	1.12
C_4H_{10}	Eq. (14)[d]	4.08	37.3	3.79	44.3	1.12	1.13	1.13
	Eq. (14)[e]	4.07	37.1	3.79	44.3	1.11	1.12	1.13
	Eq. (16)	4.06–4.09	37.9–36.7	3.79	44.3	1.11	1.12	1.13
C_6H_{14}	Eq. (14)[d]	4.32	45.1	4.04	51.9	1.11	1.12	1.12
	Eq. (16)	4.35–4.43	43.9–42.5	4.04	51.9	1.12	1.14	1.17

[a]For the exp/6 intermolecular potential

[b]Via Eq. (13)

[c]From Refs. 15 and 24

[d]Anti conformer

[e]Gauche conformer

Table 5. Calculated Lennard-Jones parameters compared with tabulated values and relative collision rates for several intermolecular potentials for small targets + He[a]

		Calculated		Tabulated[b]		z_{calc}/z_{tab}		
Target	PES	σ, Å	ε, cm^{-1}	σ, Å	ε, cm^{-1}	300 K	1500 K	3000 K
H	exp/6	2.92	3.67	2.31	26.7	1.15	1.23	1.26
	MP2/A'DZ	3.37	2.89	2.31	26.7	1.48	1.60	1.63
	MP2/CBS	3.35	2.32	2.31	26.7	1.42	1.54	1.58
	QCISD(T)/CBS	3.17	4.49	2.31	26.7	1.39	1.48	1.51
H_2	exp/6	3.01	6.58	2.75	13.7	1.06	1.09	1.10
	MP2/A'DZ	3.14	5.81	2.75	13.7	1.13	1.16	1.18
	MP2/CBS	3.07	6.64	2.75	13.7	1.11	1.14	1.15
	QCISD(T)/CBS	2.98	9.55	2.75	13.7	1.11	1.12	1.13
C	exp/6	3.08	16.0	2.94	18.8	1.07	1.08	1.08
	MP2/A'DZ	2.58	45.5	2.94	18.8	0.92	0.88	0.87
	MP2/CBS	2.57	39.3	2.94	18.8	0.88	0.85	0.84
	QCISD(T)/CBS	2.91	19.5	2.94	18.8	0.99	0.99	0.98
CH	exp/6	3.15	17.7	2.67	19.9	1.37	1.38	1.38
	MP2/A'DZ	3.10	26.9	2.67	19.9	1.44	1.42	1.41
	MP2/CBS	3.09	21.1	2.67	19.9	1.36	1.36	1.36
	QCISD(T)/CBS	3.02	26.9	2.67	19.9	1.36	1.34	1.34
$^3CH_2$	exp/6	3.21	19.2	3.19	26.6	0.95	0.97	0.97
	MP2/A'DZ	3.49	13.6	3.19	26.6	1.06	1.09	1.10
	MP2/CBS	3.47	9.72	3.19	26.6	0.99	1.03	1.04
	QCISD(T)/CBS	3.35	14.4	3.19	26.6	0.99	1.01	1.02
$^1CH_2$	exp/6	3.21	19.2	3.19	26.6	0.95	0.97	0.97
	MP2/A'DZ	3.40	20.2	3.19	26.6	1.08	1.09	1.10
	MP2/CBS	3.36	16.1	3.19	26.6	1.01	1.03	1.04
	QCISD(T)/CBS	3.29	18.9	3.19	26.6	1.00	1.02	1.02
O	exp/6	N/A						
	MP2/A'DZ	2.87	21.5	2.66	19.9	1.14	1.14	1.14
	MP2/CBS	2.79	12.7	2.66	19.9	1.01	1.03	1.04
	QCISD(T)/CBS	2.73	18.8	2.66	19.9	1.04	1.04	1.04
OH	exp/6	N/A						
	MP2/A'DZ	2.89	27.3	2.66	19.9	1.25	1.23	1.23
	MP2/CBS	2.89	16.7	2.66	19.9	1.14	1.14	1.15
	QCISD(T)/CBS	2.80	24.0	2.66	19.9	1.15	1.14	1.13
H_2O	exp/6	N/A						
	MP2/A'DZ	3.12	29.6	2.59	53.1	1.28	1.32	1.34
	MP2/CBS	3.14	14.1	2.59	53.1	1.13	1.21	1.23
	QCISD(T)/CBS	3.02	21.7	2.59	53.1	1.13	1.18	1.20

[a]Calculated via Eq. (14)

[b]From Ref. 15

Table 6. Calculated Lennard-Jones parameters for several small targets + He[a]

	Calculated		Tabulated[b]		z_{calc}/z_{tab}		
Target	σ, Å	ε, cm^{-1}	σ, Å	ε, cm^{-1}	300 K	1500 K	3000 K
H	3.35	2.32	2.31	26.7	1.42	1.54	1.58
H_2	3.07	6.64	2.75	13.7	1.11	1.14	1.15
C	2.57	39.3	2.94	18.8	0.88	0.85	0.84
CH	3.09	21.1	2.66	19.9	1.36	1.36	1.36
$^3CH_2$	3.47	9.72	3.19	26.6	0.99	1.03	1.04
$^1CH_2$	3.36	16.1	3.19	26.6	1.01	1.03	1.04
CH_3	3.48	11.3	3.19	26.6	1.02	1.06	1.07
CH_4	3.41	14.9	3.13	28.7	1.05	1.08	1.09
C_2	3.35	23.1	3.10	21.9	1.18	1.18	1.18
C_2H	3.52	16.0	3.34	32.1	0.97	1.00	1.01
C_2H_2	3.55	16.8	3.34	32.1	1.00	1.03	1.04
C_2H_3	3.64	15.8	3.34	32.1	1.04	1.08	1.10
C_2H_4	3.65	17.5	3.27	37.2	1.07	1.11	1.12
C_2H_5	3.72	17.7	3.44	35.3	1.02	1.06	1.07
C_2H_6	3.73	19.8	3.40	36.8	1.07	1.10	1.11
O	2.79	12.7	2.66	19.9	1.01	1.03	1.04
OH	2.89	16.7	2.66	19.9	1.14	1.14	1.15
H_2O	3.14	14.1	2.59	53.1	1.13	1.21	1.23
O_2	3.13	18.3	3.02	23.0	1.03	1.04	1.04
HO_2	3.20	19.8	3.02	23.0	1.10	1.10	1.11
H_2O_2	3.26	21.6	3.02	23.0	1.15	1.16	1.16
CO	3.33	14.7	3.14	22.5	1.04	1.06	1.06
HCO	3.37	16.5	3.08	49.5	0.96	1.02	1.03
H_2CO	3.35	20.5	3.08	49.5	0.99	1.03	1.05
H_3CO	2.95	27.9	3.27	46.3	0.73	0.75	0.76
CH_2OH	3.54	17.6	3.13	45.3	1.06	1.11	1.12
CH_3OH	3.48	21.1	3.10	48.7	1.07	1.11	1.12
CO_2	3.30	25.0	3.17	34.7	1.01	1.03	1.03
C_2O	3.32	30.7	3.20	33.8	1.05	1.06	1.06
HCCO	3.57	22.1	2.54	27.2	1.90	1.92	1.93
CH_2CO	3.55	24.3	3.27	46.3	1.03	1.07	1.08
CH_3CO	3.75	19.2	3.27	46.3	1.10	1.15	1.16
CH_2CHO	3.68	21.0	3.27	46.3	1.08	1.12	1.14
CH_3CHO	3.71	22.8	3.27	46.3	1.12	1.16	1.17

[a]Calculated via Eq. (14) and using the MP2/CBS intermolecular potential

[b]From Ref. 15

Figure Captions

Fig. 1. Isotropically averaged intermolecular potentials for three normal alkanes in He. The circles are the results of Eq. (9) for the exp/6 potential. The solid lines show Lennard-Jones curves based on the calculated parameters. The dotted lines show the minimum and maximum sampled energies along *r*. Two sets of results are shown for butane: one for the anti conformer equilibrium geometry (black) and one for the gauche conformer equilibrium geometry (blue).

Fig. 2. Anisotropic exp/6 intermolecular potentials for three normal alkanes in He. The lines show one-dimensional center-of-mass cuts for 20 different orientations. The circles indicate the local minima obtained via Eq. (14). The triangles indicate local minima from 20 full-dimensional trajectories. The initial conditions for the one-dimensional minimizations and for the trajectory results shown here are not related.

Figure 1

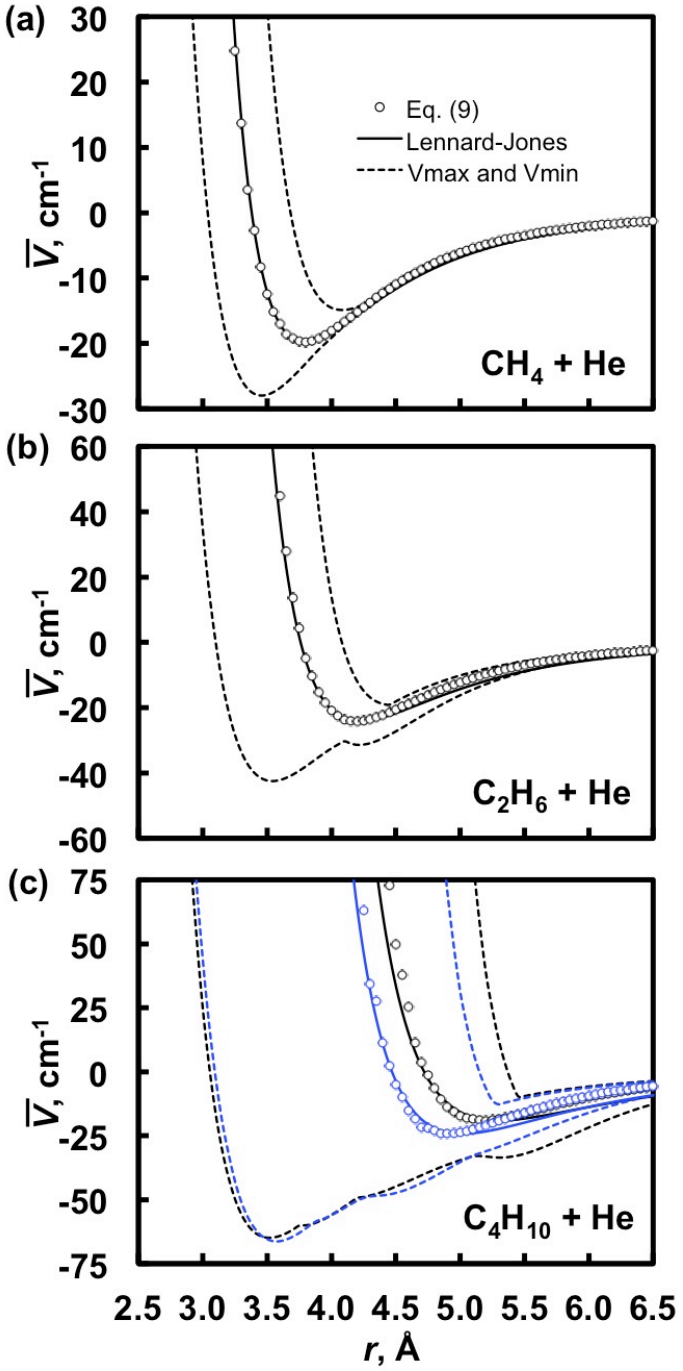

Fig. 1. Isotropically averaged intermolecular potentials for three normal alkanes in He. The circles are the results of Eq. (9) for the exp/6 potential. The solid lines show Lennard-Jones curves based on the calculated parameters. The dotted lines show the minimum and maximum sampled energies along *r*. Two sets of results are shown for butane: one for the anti conformer equilibrium geometry (black) and one for the gauche conformer equilibrium geometry (blue).

Figure 2

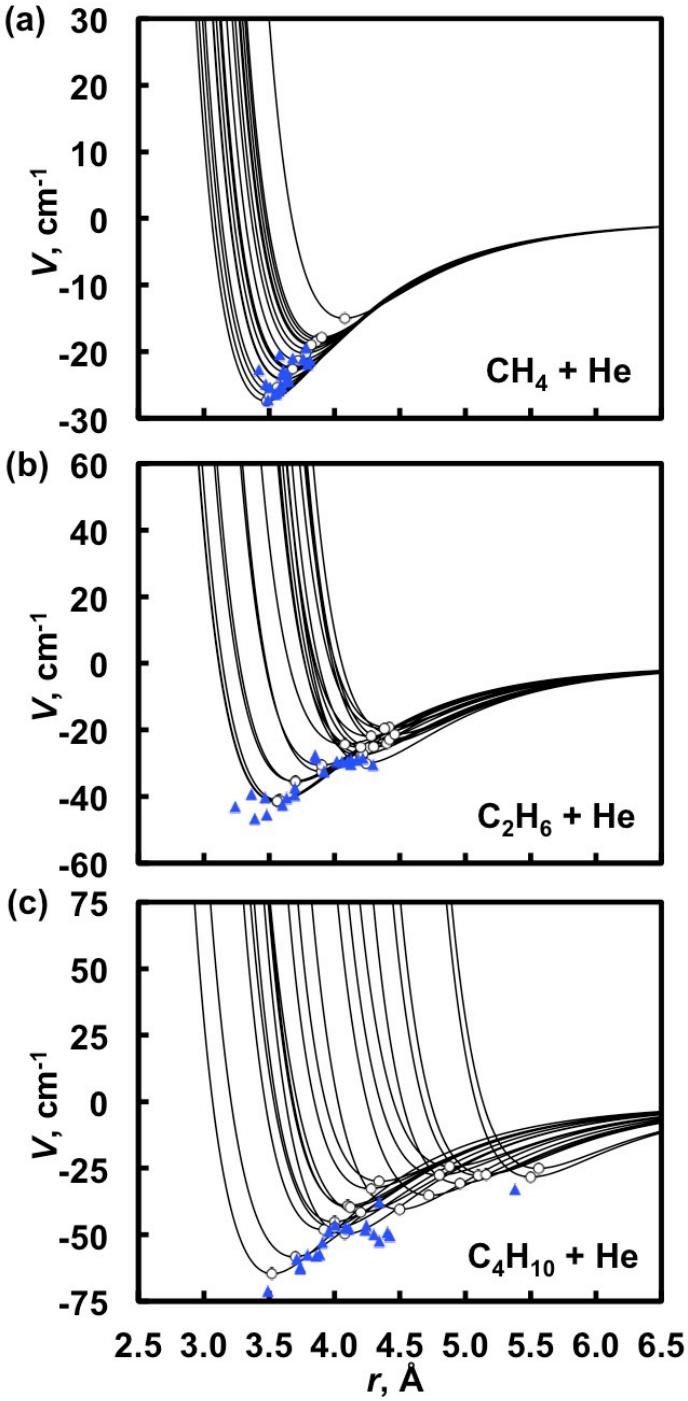

Fig. 2. Anisotropic exp/6 intermolecular potentials for three normal alkanes in He. The lines show one-dimensional center-of-mass cuts for 20 different orientations. The circles indicate the local minima obtained via Eq. (14). The triangles indicate local minima from 20 full-dimensional trajectories. The initial conditions for the one-dimensional minimizations and for the trajectory results shown here are not related.

References

[1] G. C. Maitland, M. Rigby, E. B. Smith, and W. A. Wakeham, Intermolecular Forces: Their Origin and Determination (Clarendon, Oxford, 1987).

[2] J. O. Hirschfelder, C. F. Curtiss, R. B. Bird, R. B. Molecular Theory of Gases and Liquids (Wiley, New York, 1954), pp. 1110, 1212.

[3] N. J. Brown, L. A. J. Bastian, and P. N. Price, Prog. Energy Combust. Sci. 37 (2011) 565.

[4] A. W. Jasper and J. A. Miller, J. Phys. Chem. A 113 (2009) 5612.

[5] A. W. Jasper and J. A. Miller, J. Phys. Chem. A 115 (2011) 6438.

[6] J. Troe, J. Chem. Phys. 66 (1977) 4745. J. Troe, J. Chem. Phys. 66 (1977) 4758.

[7] T. Baer and W. L. Hase, Unimolecular Reaction Dynamics: Theory and Experiments (Oxford University Press, New York, 1996).

[8] N. J. Brown and J. A. Miller, J. Chem. Phys. 80 (1984) 5568.

[9] A. Fernandez-Ramos, J. A. Miller, S. J. Klippenstein, and D. G. Truhlar, Chem. Rev. 106 (2006) 4578.

[10] P. J. Dagdigian and M. H. Alexander, J. Chem. Phys. 137 (2012) 094306.

[11] P. J. Dagdigian and M. H. Alexander, J. Chem. Phys. 138 (2013) 164305.

[12] L. Monchick and S. Green, J. Chem. Phys. 63 (1975) 2000.

[13] P. Middha, B. Yang, and H. Wang, Proc. Combust. Inst. 29 (2002) 1361.

[14] P. H. Paul and J. Warnatz, Proc. Combust. Inst. 27 (1998) 495.

[15] R. J. Kee, F. M. Rupley, J. A. Miller, M. E. Coltrin, J. F. Grcar, E. Meeks, H. K. Moffat, A. E. Lutz, G. Dixon-Lewis, M. D. Smooke, J. Warnatz, G. H. Evans, R. S. Larson, R. E. Mitchell, L. R. Petzold, W. C. Reynolds, M. Caracotsios, W. E. Stewart, P. Glarborg, C. Wang, C. L. McLellan, O. Adigun, W. G. Houf, C. P. Chou, S. F. Miller, P. Ho, P. D. Young, D. J. Young, D. W. Hodgson, M.V. Petrova, K. V. Puduppakkam, CHEMKIN, Reaction Design, San Diego, CA, 2010.

[16] Quantum mechanically there is some distribution of geometries associated with the zero point wave function even at 0 K.

[17] H. C. Andersen, J. Chem. Phys. 7 (1979) 1.

[18] A. W. Jasper and N. Hansen, Proc. Combust. Inst. 34 (2013) 279.

[19] N. Taxman, Phys. Rev. 110 (1958) 1235.

[20] K. Chae, P. Elvati, and A. Violi, J. Phys. Chem. B 115 (2011) 500.

[21] Y. Wang, H. C. Mak, Chem. Phys. Lett. 235 (1995) 37. Liu, T.; Truhlar, D. G. TB, version 1.0.1, University of Minnesota: Minnesota, 2004, see comp.chem.umn.edu/tbpac. Liu, T. Ph.D. Thesis, University of Minnesota, 2000.

[22] W. A. Alexander and D. Troya, J. Phys. Chem. A, 110 (2006) 10834.

[23] J. O. Hirschfelder, C. F. Curtiss, and R. B. Bird, Molecular Theory of Gases and Liquids (Wiley, New York, 1954), pp. 1110, 1212.

[24] L. S. Tee, S. Gotoh, and W. E. Stewart, I&EC Fundamentals 5 (1966) 356.

[25] L. A. J. Bastien, P. N. Price, and N. J. Brown, Int. J. Chem. Kin. 42 (2010) 713.

[26] J. Klimeš and A. Michaelides, J. Chem. Phys. 137 (2012) 120901.

[27] J. Řezác and P. Hobza, J. Chem. Theory Comput. 9 (2013) 2151.